Check for updates

Singlet oxygen formation in bio-inspired synthesis of a hollow Ag@AgBr photocatalyst for microbial and chemical decontamination†

S. Zhang,[a] H. Zhang,[b] S. Wang, iD *[b] L. Liu iD *[b] and S. Liu iD [b]

Hollow Ag@AgBr nanospheres were prepared using a greener version of a microbial process starting with AgCl colloid formation in a yeast extract (YE) and peptone solution. The Kirkendall effect has been exploited to obtain the unique Ag@AgBr heterostructures for excellent solar light–induced oxidizing properties against both microbial and chemical contaminants. Singlet oxygen generation was confirmed by electron spin resonance studies.

Worldwide, the improper disposal of wastewater and sludge has resulted in the pollution of numerous water resources with both hazardous chemicals and pathogenic microbes. A particular concern in many developing countries has been microbial contamination. To get safe drinking water, chlorination is the most widely used wastewater treatment method. However, the toxic disinfection by-products (DBPs) formed in chlorinated wastewaters may have an adverse impact on aquatic organisms.[1] Photocatalysis is an alternative process that can be used in water purification.[2,3] A great amount of research in the solar-light-driven catalysis field has been aimed at developing semiconductor nanomaterials, such as TiO_2, which not only decompose toxic organic compounds but also kill bacteria.[4,5] Reactive oxygen species (ROS) formed during a photocatalytic process are reported to be nonselective oxidizing agents for many organic pollutants. Similarly, ROS can kill pathogens by causing oxidative damage to essential bio-macromolecules.[6] Studies on Ag^0-containing silver halides (Ag@AgX, X = Cl, Br, I) have confirmed that these plasmonic photocatalysts could effectively harness the energy in photons from the visible range to generate ROS.[7–11] Coactively, the Ag^+ released from Ag@AgX could bind to DNA and other sulphur-, nitrogen- and phosphorus-containing components, followed by damaging

bacterial cells with multiple modes from interfering with DNA replication to inactivating respiratory enzymes.[12,13] Therefore, the exploration of multifunctional Ag@AgX nanohybrids for environmental applications has witnessed exciting advancements over the past decade.

We have successfully synthesized Ag@AgCl in aqueous LB broth (Miller's) solution at room temperature with 5 min sunlight exposure. The yeast extract (YE) and peptone used as amino acid sources in the microbiological culture media, which contain Ag-bound histidine and the electron donor tyrosine, were identified as key components in facilitating the formation of Ag@AgCl.[14–16] The broth alone strategy dramatically simplifies the conventional microbial process by cutting the use of microorganisms and thus provides a greener way for nanomaterial preparation. Moreover, the biogenic Ag@AgCl outperforms commercial TiO_2 in decomposing organic dyes under solar light with excellent photocatalytic stability. Based on these works, we attempted to fabricate high quality hollow Ag@AgBr nanostructures for water remediation, since hollow structural materials usually show improved catalytic properties due to their high surface area, low density, and porous structure. The enhancement is achieved by allowing greater light absorption/reflection into the interior and increasing mass transfer as well as providing more reaction sites.[17,18]

Different from the template-assisted synthesis of hollow/porous AgBr/Ag composites,[19–21] our nano Ag-incorporated $AgCl_xBr_{1−x}$ has been obtained by the precipitation of $AgNO_3$ with sodium chloride in peptone solution first, followed by the nanoscaled Kirkendall process (the ion-exchange reaction between $Br^−$ and AgCl due to the large difference between the solubility of AgBr and AgCl) and 5 min solar light irradiation. Peptone is produced by the partial hydrolysis of animal tissues, milk, plants or microbial cultures. NaCl is usually formed during the neutralization of acid hydrolysis, resulting in a product with a medium to high salt content. The photocatalytic activities of the Ag@AgBr nanocrystals were evaluated for methyl orange (MO) degradation and *E. coli*

---

[a] *Department of Orthopaedics, First Hospital of Jilin University, China*
[b] *Department of Chemical Engineering, Curtin University, Perth, Western Australia 6845, Australia. E-mail: shaobin.wang@curtin.edu.au, lihong.liu@curtin.edu.au*

This journal is © The Royal Society of Chemistry 2017

Catal. Sci. Technol., 2017, **7**, 4355–4360 | 4355

disinfection. Electron spin resonance (ESR) spectroscopy was employed to study the ROS involved in the reaction. Except for the well-recognized $^{\cdot}$OH and $O_2^{\cdot-}$,[22] singlet oxygen ($^{1}O_2$) was directly identified for the first time as a contributor to the degradation of pollutants using Ag@AgBr catalysts.

Structure and morphology characterization of Ag@AgCl$_x$Br$_{1-x}$ nanocrystals

Fig. 1a shows the XRD patterns of nanocrystals synthesized with different concentrations of Cl$^-$. The Ag@AgCl sample exhibits diffraction peaks at 27.9°, 32.3°, 46.3°, 54.9°, 57.5°, and 67.4°, corresponding to the (111), (200), (220), (311), (222), and (400) planes of face-centered cubic (fcc) phase AgCl (JCPDS file: 31-1238).[23] The diffraction peaks of Ag@AgBr at 26.7°, 31.0°, 44.4°, 52.6°, 55.0°, 64.5° and 73.3° can be indexed to the (111), (200), (220), (311), (222), (400), and (420) planes of cubic phase AgBr (JCPDS file: 06-438).[24] There are no obvious peaks of metallic Ag due to the small size of the photo-reduced Ag NPs. Interestingly, Ag@AgCl$_{0.64}$Br$_{0.36}$ and Ag@AgCl$_{0.36}$Br$_{0.64}$ particles display a pure phase of fcc lattice close to Ag@AgBr. Changing the composition from chloride-rich to bromide-rich causes a monotonic peak shift towards smaller angles. Our results indicate that, in the presence of yeast extract and peptone, the co-precipitation of Ag$^+$ between Cl$^-$/Br$^-$ leads to the formation of a homogeneous solid solution phase of AgCl and AgBr. This result is consistent with previous experimental works.[25]

The optical properties of the synthesized nanostructures were determined using UV-vis absorption spectroscopy. As shown in Fig. 1b, owing to the surface plasmonic resonance effect of the nano Ag, all Ag@AgCl$_x$Br$_{1-x}$ samples show stronger absorption in the visible region than AgCl; with increasing [Br$^-$], the absorption peak at 266 nm corresponding to the direct bandgap of AgCl was gradually replaced by a stronger peak at 321 nm associated with the direct bandgap of AgBr.

The particle z-average sizes and polydispersity index (PDI) were obtained by DLS measurements (Table S1†). Two nano silver-incorporated AgCl and AgBr samples had z-average diameters around 120 nm. At 25 °C, the solubility product constants (K_{sp} values) of AgBr and AgCl are 5.0×10^{-13} and 1.8×10^{-10}, respectively. The nucleation of AgBr is faster; therefore one would expect two different populations of AgBr and AgCl in the Ag@AgCl$_{0.36}$Br$_{0.64}$ and Ag@AgCl$_{0.64}$Br$_{0.36}$ samples, but the PDI of these mixed silver halide particles was very low (<0.1). This supports the homogeneity of the XRD results in Fig. 1a.

Representative FESEM images of Ag@AgCl and Ag@AgBr (Fig. 2a–d) reveal that these spherical samples were approximately 110 nm in diameter. Solid Ag@AgCl with a relatively wide size distribution is roughly covered with tiny silver nanoparticles (indicated by white arrows). The hollow nature of Ag@AgBr nanostructures is clearly shown in Fig. 2d. The average pore diameter determined based on the desorption of nitrogen was approximately 8.7 nm. The BET measurement revealed that the as-synthesized Ag@AgBr had a surface area of 5.98 m^2 g^{-1}, which is comparable to previously reported data.[26] It is difficult to obtain a high quality TEM image of Ag@AgBr due to the problem with fast reduction of AgBr NPs by the electron beam of TEM. Fig. 2e shows a HAADF-STEM image of Ag@AgBr NPs and the corresponding EDX maps. In contrast to most hollow Ag decorated halides obtained by NaBH$_4$ reduction which are Ag-rich on the surface,[18] here, the EDX elemental maps show pronounced Br signals at the outermost parts of the particles.

Based on the above-mentioned results, we propose a possible reaction route and the structural evolution of the hollow spheres, as shown in Scheme 1. The first step is the instantaneous formation of AgCl nuclei after mixing AgNO$_3$ with a YE and peptone solution. With the help of biomolecules provided by YE and peptone, the nuclei aggregate into well-dispersed solid AgCl nanospheres with a diameter around 120 nm (Table S1†). The introduction of NaBr leads to the surface conversion of AgCl to AgBr driven by the decrease in enthalpy of precipitation of the silver halides.[27] Because Ag$^+$ cations diffused outward more quickly than Br$^-$ diffused inward, nanoscaled Kirkendall voids were generated near the AgCl/AgBr interface.[19,28] Upon solar light irradiation, AgBr is

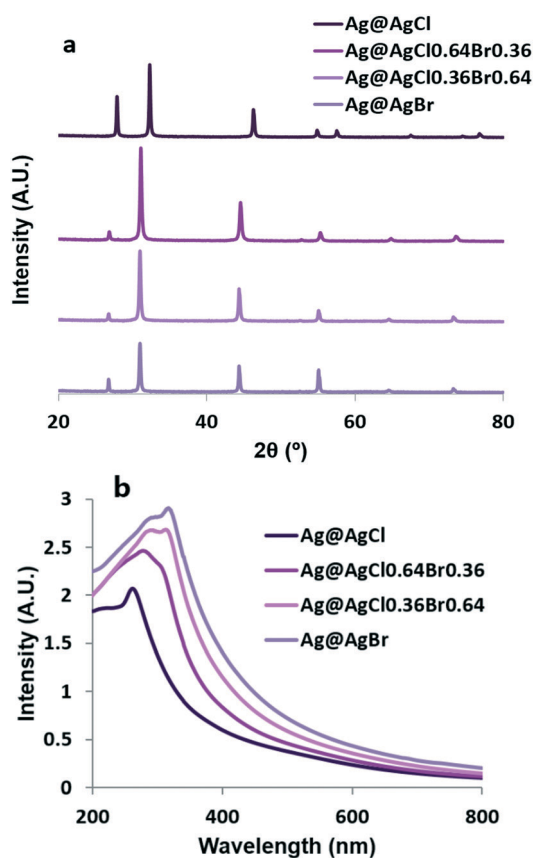**Fig. 1** (a) XRD patterns and (b) UV-vis absorption spectra of Ag@AgCl$_x$Br$_{1-x}$ (x = 1, 0.64, 0.36 and 0) nanocrystals.

4356 | Catal. Sci. Technol., 2017, 7, 4355–4360

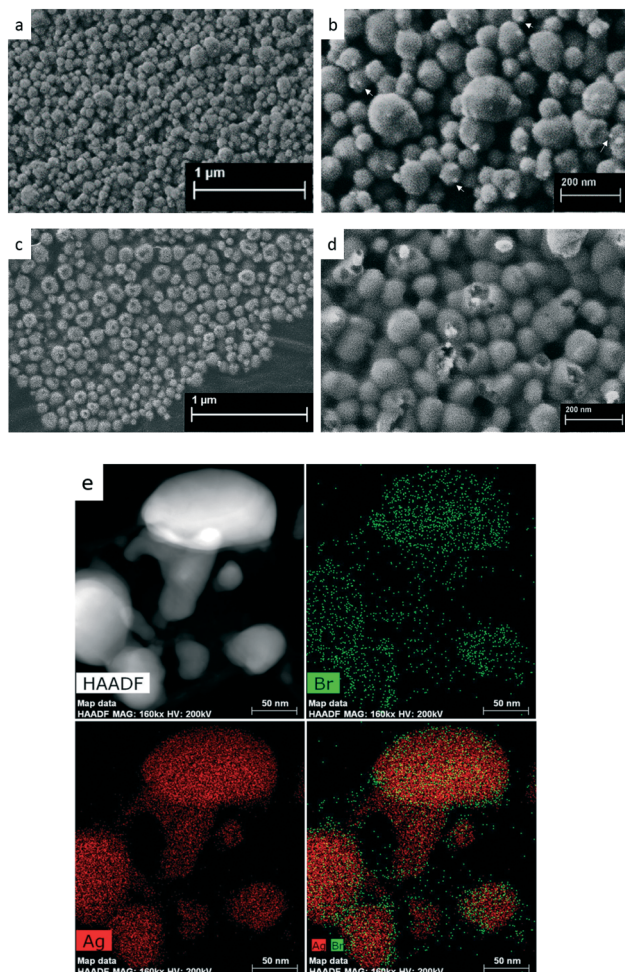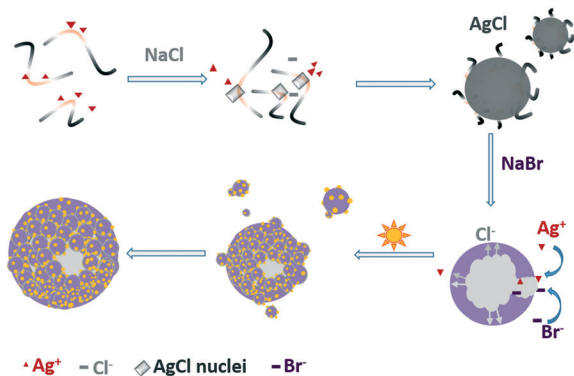This journal is © The Royal Society of Chemistry 2017

Fig. 2 Morphological images of Ag@AgCl (a and b) and Ag@AgBr (c and d). (e) HAADF-STEM image and the corresponding HAADF-STEM-EDS maps of different elements, showing the distribution of Ag and Br elements in Ag@AgBr.

UV exposure. The Ag NPs are able to absorb visible light and drive a collective and coherent oscillation of the electrons with the incident photons due to the localized surface plasmon resonance (LSPR). The decay of LSPR or the electron–phonon relaxation is generally coupled with the vibrations of the Ag and AgBr lattices and heating of the surrounding local environment. An extremely high transient temperature of the irradiation location promoted the Ostwald ripening process by enhancing the dissolution rate of smaller AgBr nanoparticles.[14]

Photocatalytic activities of Ag@AgCl$_x$Br$_{1-x}$ nanoparticles

The photocatalytic efficiency of the samples was evaluated by studying the degradation of methyl orange (MO) dye. Fig. 3 shows the variation of MO characteristic peak intensity as a function of irradiation time. After the adsorption–desorption process in the dark for 30 min, the change in the concentration of MO molecules was monitored by measuring the absorbance at 463 nm. The adsorption fraction of MO on the photocatalyst was given by (A1 − A2)/A1, where A1 is the absorption of 10 ppm MO solution and A2 is the absorption of the dye solution after reaching equilibrium. The accumulation of MO on the hollow Ag@AgBr particles was 7%. It is known that an appropriate adsorption capacity of photocatalysts is beneficial to the catalytic activity.[29] Under solar light, Ag@AgCl decomposed 47% of MO after 8 min irradiation. The photocatalytic degradation rate was enhanced by tuning the composition from Cl⁻ rich to Br⁻ rich, as 71% and 76% MO were decomposed by Ag@AgCl$_{0.64}$Br$_{0.36}$ and Ag@AgCl$_{0.36}$Br$_{0.64}$, respectively. The Ag@AgBr sample exhibits the highest photocatalytic degradation efficiency, and 81.0% of MO could be degraded within 8 min. For comparison, Ag@AgBr particles prepared in deionized (DI) water (named Ag@AgBr-DI) without yeast extract and peptone involvement was evaluated for the degradation of various dyes under visible light irradiation. Ag@AgBr-DI exhibited a much lower photocatalytic performance, as shown in Fig. S1.†

To evaluate the durability of the catalysts, three successive methyl orange degradation tests under solar light were
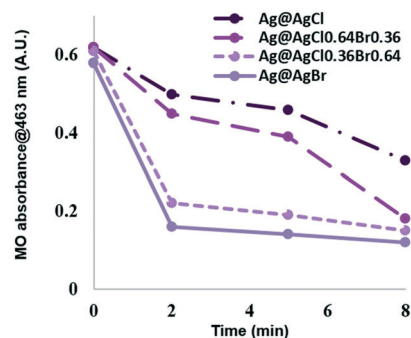
excited to generate electrons at the conduction band and then react with Ag⁺ to form Ag NPs across the surface. Meanwhile, biomolecules like peptide or DNA adsorbed on AgBr might facilitate the cleavage of AgBr NPs due to high energy

Scheme 1 Illustration of the conversion process from a solid AgCl colloid to hollow Ag@AgBr particles through the Kirkendall effect.

Fig. 3 Methyl orange degradation rate using nano Ag-incorporated silver halide samples.

This journal is © The Royal Society of Chemistry 2017

Catal. Sci. Technol., 2017, **7**, 4355–4360 | **4357**

carried out and the removal of the dye was still 90% after two times of recycling. Additionally, as shown in Fig. S2,† even after exposure to sunlight for 1 hour, the XRD patterns of Ag@AgBr particles showed no apparent change. The photocatalytic stability of Ag@AgBr may be ascribed to the electron confining property of plasmonic Ag NPs that prevents photolysis of AgBr to Ag nanoclusters.[14]

Antimicrobial test

Silver-based antimicrobial agents are gaining tremendous attention in various fields due to their broad spectrum activity, efficacy and low cost. Many studies have suggested that both dissolved and nanoparticulate silver contribute to the biocidal property of Ag materials, with Ag^+ as the main germicidal source.[30,31] However, free Ag^+ has ample opportunities to react with Cl^-, SO_4^{2-}, and CO_3^{2-} in the culture media and the wastewater, which therefore gave rise to changes in its potency.[32] Moreover, under different lighting conditions, bacterial cells exhibited variable susceptibility to Ag^+.[33] As shown in Fig. 4A and C, the biocidal activities of the Ag chlorobromides were evaluated by testing the growth inhibition concentrations against *E. coli* in the dark first. The MIC for the silver ions was determined to be 3.12 ppm against *E. coli*, which matched well with previous studies.[13] The growth of *E. coli* was inhibited by Ag@AgCl and Ag@AgBr at 6.25 and 12.5 ppm, respectively. The formation of solid Ag@AgX and Ag NPs on the surface of Ag@AgCl$_x$Br$_{1-x}$ hindered the elution of Ag^+ from the particles, resulting in lower $[Ag^+]$ and *E. coli* being less sensitive to Ag@Ag chlorobromides in the solution.[34] After exposing the plates to solar light for 30 min, a reverse trend was observed with the MIC values: Ag@AgBr (6.25 ppm) < Ag@AgCl (12.5 ppm) < $AgNO_3$ (25 ppm). The enhanced antibacterial ability of Ag@AgBr could be attributed to the synergistic action of free radicals, such as $^{\bullet}OH$ and $O_2^{\bullet-}$, and photogenerated holes (h^+) on the surface of photocatalysts.[8] These oxidizing agents do not have specificity towards microbial cells when compared with mammalian cells.[35] In contrast, another kind of ROS, singlet oxygen ($^1O_2$), is more toxic to prokaryotic cells than to eukaryotic cells.[36] Moreover, $^1O_2$ is one of the most acutely lethal ROS to bacterial cells because no enzyme can detoxify it. Using chemiluminescence photometry and near-infrared emission techniques, singlet oxygen formation on a TiO_2 catalyst has been well studied by Nosaka's group.[37–39] In this study, ESR spectroscopy combined with 2,2,6,6-tetramethyl-4-piperidinol (TMP) was employed to probe the generation of $^1O_2$, since the specific $^1O_2$ oxidation of TMP to the 2,2,6,6-tetramethyl-4-piperidinol-*N*-oxyl radical (TMPN) was detectable by ESR.[40]

As shown in Fig. 5a, the time-dependent increase in ESR signal was obvious following the irradiation of TMP in the presence of Ag@AgBr. The characteristic 1:1:1 triplet could be unequivocally attributed to TMPN. The signal intensity of TMPN was decreased after adding methyl orange, indicating the competitive consumption of $^1O_2$ by MO molecules.

Garg *et al.* have determined the main reactive species produced on irradiation of AgCl(s) and proposed the $^1O_2$ generation as a result of H_2O_2 reaction with free chlorine (OCl^-).[41] It has been known that the yield of singlet oxygen is 76% with H_2O_2 and hypobromite.[42] Based on previous works, we propose the following $^1O_2$ generation process. Eqn (1) describes the absorption of a photon by a Ag@AgBr crystal and the creation of a positive hole in the valence band and an electron in the conduction band. The electrons tend to move to the silver nanoparticles on the surface and may react with O_2 to give a superoxide anion and the more stable H_2O_2 (eqn (2) and (3)). On the other hand, bromide ions (Br^-) may capture the photogenerated hole on the irradiated AgBr to form a bromine atom. This species then reacts rapidly with bromide to produce $Br_2^{\bullet-}$. Two of such anion radicals disproportionate to give bromine (Br_2) and subsequently hydrolyze to form
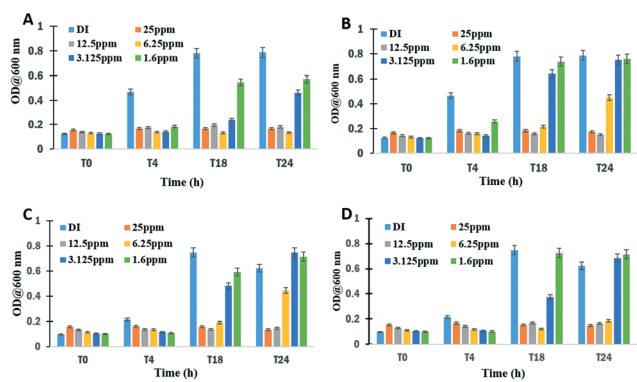

Fig. 4 Minimum inhibitory concentration (MIC) evaluation of Ag@AgCl (A and B) and Ag@AgBr (C and D) samples.
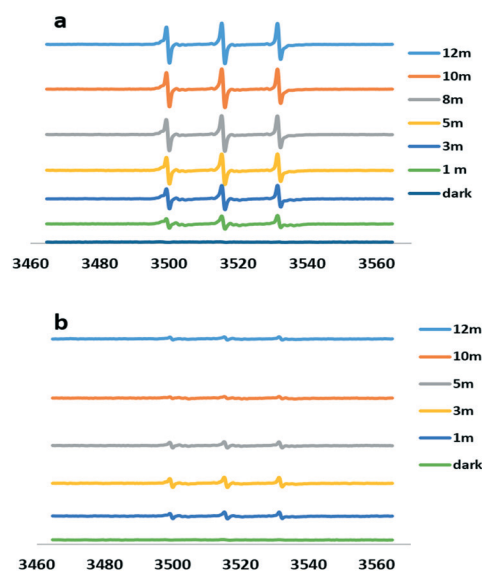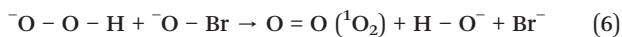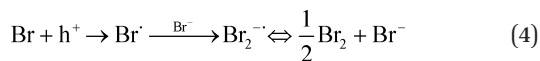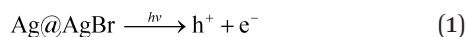

Fig. 5 Electron spin resonance spectra of aqueous suspensions of Ag@AgBr with TMP only (a) and with TMP plus methyl orange (b) after 12 min light irradiation.

4358 | *Catal. Sci. Technol.*, 2017, **7**, 4355–4360

This journal is © The Royal Society of Chemistry 2017

OBr$^-$ (eqn (4) and (5)).[43] Finally, the reaction of H_2O_2 and OBr$^-$ results in the formation of singlet oxygen ($^1\Delta g$) O=O (ref. 44) as a powerful bactericidal ROS.[45]

$$Ag@AgBr \xrightarrow{h\nu} h^+ + e^- \tag{1}$$

$$Ag^0(e^-) + O_2 \rightarrow {}^\bullet O_2{}^- \tag{2}$$

$${}^\bullet O_2{}^- + {}^\bullet O_2{}^- \rightarrow H_2O_2 \tag{3}$$

$$Br + h^+ \rightarrow Br^\bullet \xrightarrow{Br^-} Br_2{}^{\bullet-} \Leftrightarrow \frac{1}{2}Br_2 + Br^- \tag{4}$$

$$Br_2 + H_2O \rightarrow OBr^- \tag{5}$$

$$^-O - O - H + {}^-O - Br \rightarrow O = O\,(^1O_2) + H - O^- + Br^- \tag{6}$$

$^1O_2$ is highly electrophilic and reacts rapidly with amines, unsaturated carbon–carbon bonds and sulfides.[46] These substrates are relevant to bacterial biomolecules such as the protein/peptidoglycan of the cell wall, unsaturated phospholipids within the cytoplasm membrane, enzymes and nucleic acids. The oxidative degradation of cellular constituents leads to bacterial death.[47]

Considering the wide application of Ag@AgBr on various supports,[48–53] our study provides a facile way to construct tertiary or even more complicated hybrid materials.

Conclusions

Ag@AgBr hollow spheres with a diameter around 110 nm were successfully synthesized using a simplified microbial method with the Kirkendall effect. The Ag@AgBr NPs are promising composites in practical fields for water purification. Singlet oxygen generation from Ag@AgBr was detected for the first time by ESR study. Since $^1O_2$ specifically targets microorganisms over host mammalian cells, Ag@AgBr can be exploited in photodynamic therapy for the topical treatment of infections.

Conflicts of interest

There are no conflicts to declare.

Acknowledgements

References

1 K. Watson, G. Shaw, F. D. Leusch and N. L. Knight, *Water Res.*, 2012, **46**, 6069.

2 M. Chong, B. Jin, C. Chow and C. Saint, *Water Res.*, 2010, **44**, 2997.

3 J. Ke, J. Liu, H. Sun, H. Zhang, X. Duan, P. Liang, X. Li, M. Tade, S. Liu and S. Wang, *Appl. Catal., B*, 2017, **200**, 47.

4 J. Chen, M. Liu, L. Zhang, J. Zhang and L. Jin, *Water Res.*, 2003, **37**, 3815.

5 S. Ma, S. Zhan, Y. Jia and Q. Zhou, *ACS Appl. Mater. Interfaces*, 2015, **7**, 21875.

6 S. Malato, P. Fernandez-Ibanez, M. I. Maldonado, J. Blanco and W. Gernjak, *Catal. Today*, 2009, **147**, 1.

7 P. Wang, B. Huang, X. Zhang, X. Qin, Y. Dai, Z. Wang and Z. Lou, *ChemCatChem*, 2011, **3**, 360.

8 Y. Hou, X. Li, Q. Zhao, G. Chen and C. L. Raston, *Environ. Sci. Technol.*, 2012, **46**, 4042.

9 C. An, J. Wang, C. Qin, W. Jiang, S. Wang, Y. Li and Q. Zhang, *J. Mater. Chem.*, 2012, **22**, 13153.

10 Z. Wang, J. Liu and W. Chen, *Dalton Trans.*, 2012, **41**, 4866.

11 J. Song, I. Lee, J. Roh and J. Jang, *RSC Adv.*, 2014, **4**, 4558.

12 L. Liu, Y. Chen, J. Liang and S. Liu, *Biointerface Res. Appl. Chem.*, 2014, **4**, 741.

13 P. Suchomel, L. Kvitek, A. Panacek, R. Prucek, J. Hrbac, R. Vecerova and R. Zboril, *PLoS One*, 2015, **10**, e0119202, DOI: 10.1371/journal.pone.0119202.

14 Z. Shen, B. Liu, V. Pareek, S. Wang, X. Li, L. Liu and S. Liu, *RSC Adv.*, 2015, **5**, 80488.

15 L. Liu, T. Liu, M. Tade, S. Wang, X. Li and S. Liu, *Enzyme Microb. Technol.*, 2014, **67**, 53.

16 L. Liu, Z. Shao, H. M. Ang, M. O. Tade and S. Liu, *RSC Adv.*, 2014, **4**, 14564.

17 C. An, J. Wang, J. Liu, S. Wang and Y. Sun, *ChemSusChem*, 2013, **6**, 1931.

18 A. Shahzad, T. Yu and W. Kim, *RSC Adv.*, 2016, **6**, 54709.

19 Q. Dong, Z. Jiao, H. Yu, J. Ye and Y. Bi, *CrystEngComm*, 2014, **16**, 8317.

20 S. Lou, X. Jia, Y. Wang and S. Zhou, *Appl. Catal., B*, 2015, **176–177**, 586.

21 Y. Pang, L. Song, C. Chena and L. Ge, *Appl. Surf. Sci.*, 2017, **420**, 361.

22 C. Hu, Y. Lan, J. Qu, X. Hu and A. Wang, *J. Phys. Chem. B*, 2006, **110**, 4066.

23 A. Shahzad, W. Kim and T. Yu, *Dalton Trans.*, 2016, **45**, 9158.

24 S. Bao, Z. Wang, X. Gong, C. Zeng, Q. Wu, B. Tian and J. Zhang, *J. Mater. Chem. A*, 2016, **4**, 18570.

25 Z. Li and Y. Sun, *J. Mater. Chem. A*, 2013, **1**, 6786.

26 C. Wu, *J. Mater. Res.*, 2015, **30**, 677.

27 T. Sugimoto and K. Miyake, *J. Colloid Interface Sci.*, 1990, **140**, 335–347.

28 W. Wang, M. Dahl and Y. Yin, *Chem. Mater.*, 2013, **25**, 1179.

29 X. Zou, H. Fan, Y. Tian, M. Zhang and X. Yan, *Dalton Trans.*, 2015, **44**, 7811.

30 L. Liu, J. Yang, J. Xie, Z. Luo, J. Jiang, Y. Yang and S. Liu, *Nanoscale*, 2013, **5**, 3834.

31 M. Shen, X. Zhou, X. Yang, J. Chao, R. Liu and J. Liu, *Sci. Rep.*, 2015, **5**, 9674, DOI: 10.1038/srep09674.

32 S. Zhang, C. Du, Z. Wang, X. Han, K. Zhang and L. Liu, *Toxicol. In Vitro*, 2013, **27**, 739.

33 S. Zhang, L. Liu, V. Pareek, T. Becker, J. Liang and S. Liu, *J. Microbiol. Methods*, 2014, **105**, 42.

34 Z. Liu, W. Guo, C. Guo and S. Liu, *RSC Adv.*, 2015, **5**, 72872.

35 F. Vatansever, W. C. de Melo, P. Avci, D. Vecchio, M. Sadasivam, A. Gupta, R. Chandran, M. Karimi, N. A. Parizotto, R. Yin, G. P. Tegos and M. R. Hamblin, *FEMS Microbiol. Rev.*, 2013, **37**, 955.

36 C. Takahashi, Y. Tsujimoto and Y. Yamamoto, *J. Clin. Biochem. Nutr.*, 2012, **5**, 128.

37 T. Daimon and Y. Nosaka, *J. Phys. Chem. C*, 2007, **111**, 4420.

38 H. Saito and Y. Nosaka, *J. Phys. Chem. C*, 2014, **118**, 15656.

39 Y. Nosaka, T. Daimon, A. Y. Nosaka and Y. Murakami, *Phys. Chem. Chem. Phys.*, 2004, **6**, 2917.

40 P. Liang, C. Zhang, X. Duan, H. Sun, S. Liu, M. O. Tade and S. Wang, *ACS Sustainable Chem. Eng.*, 2017, **5**, 2693.

41 S. Garg, T. Ma, C. J. Miller and T. D. Waite, *J. Phys. Chem. C*, 2014, **118**, 26659.

42 D. F. Evans and M. W. Upton, *J. Chem. Soc., Dalton Trans.*, 1985, 1141.

43 M. A. Fox and T. L. Pettit, *J. Org. Chem.*, 1985, **50**, 5013.

44 E. Mckeown and W. A. Waters, *J. Chem. Soc. B*, 1966, 1040.

45 L. Villén, F. Manjón, D. García-Fresnadillo and G. Orellana, *Appl. Catal., B*, 2006, **69**, 1.

46 M. C. DeRosa and R. J. Crutchley, *Coord. Chem. Rev.*, 2002, **233**–**234**, 351.

47 T. Maisch, J. Baier, B. Franz, M. Maier, M. Landthaler, R. Szeimies and W. Bäumler, *Proc. Natl. Acad. Sci. U. S. A.*, 2007, **104**, 7223.

48 Y. Xu, H. Xu, J. Yan, H. Li, L. Huang, J. Xia, S. Yin and H. Shu, *Colloids Surf., A*, 2013, **436**, 474.

49 K. Li, J. Xue, Y. Zhanga, H. Wei, Y. Liu and C. Dong, *Appl. Surf. Sci.*, 2014, **320**, 1.

50 L. Jin, G. Zhu, M. Hojamberdiev, X. Luo, C. Tan, J. Peng, X. Wei, J. Li and P. Liu, *Ind. Eng. Chem. Res.*, 2014, **53**, 13718.

51 C. Shen, Q. Zhu, Z. Zhao, T. Wen, X. Wang and A. Xu, *J. Mater. Chem. A*, 2015, **3**, 14661.

52 W. Wang, H. Du, R. Wang, T. Wen and A. Xu, *Nanoscale*, 2013, **5**, 3315.

53 Q. Zhu, W. Wang, L. Lin, G. Gao, H. Guo, H. Du and A. Xu, *J. Phys. Chem. C*, 2013, **117**, 5894.